Supplementary material for: Characterising englacial R-channels using artificial moulins

Annegret Pohle,[1,2] Mauro A. Werder,[1,2] Dominik Gräff,[1,2] Daniel Farinotti[1,2]

[1] *Laboratory of Hydraulics, Hydrology and Glaciology (VAW), ETH Zurich, Switzerland*
[2] *Swiss Federal Institute for Forest, Snow and Landscape Research (WSL), Birmensdorf, Switzerland*
Correspondence: Annegret Pohle <apohle@ethz.ch>

Here we include results and detailed derivations that are not directly relevant for the presentation in the main document.

AERIAL IMAGE OF FIELD SITE

Figure S1 provides an ortho-rectified aerial image of the field site.

ABSOLUTE PRESSURE AND TEMPERATURE MEASUREMENTS

Fig. S2 shows water pressure (p_w) and water temperature (T_w) measurements at the sensors, for the times of selected tracer experiments (equivalent to Fig. 3 in the main document). Table S1 states the depths of the CTD sensors for each day of measurements.

ESTIMATION OF THE KINETIC POTENTIAL GRADIENT

The kinetic potential gradient is usually neglected in glaciological applications (e.g. Röthlisberger, 1972; Nye, 1976; Clarke, 2003). Here we estimate an upper bound of its size. The kinetic potential is defined by

$$\phi_v = \frac{\rho_w v^2}{2}, \tag{S1}$$

where v is the water flow velocity. We denote the change in velocity over the test section by Δv. The kinetic potential gradient can then be expressed in terms of Δv and the mean flow speed $\bar{v}$ as

$$\frac{\partial \phi_v}{\partial z} \approx \frac{\rho_w}{l} \Delta v \, \bar{v}. \tag{S2}$$

Now, assuming that the discharge is fixed over the test section, the change in v stems from the change in the channel cross-sectional area S. As bounds on the deviation of S from its mean value $\bar{S}$ (which is what we have from measurements), we use a factor of two; i.e. we assume that at most $S = 2\bar{S}$ and at least $S = \bar{S}/2$. For AM13, this gives a maximum $\Delta v \approx 1\,\mathrm{ms}^{-1}$ (using values of $Q \approx 0.02\,\mathrm{m}^3\mathrm{s}^{-1}$ and $\bar{S} = 0.03\,\mathrm{m}^2$), and slightly less for AM15. Using above formula (Eq. (S2)), $\Delta v = 1\,\mathrm{ms}^{-1}$ and typical values for AM13 ($\bar{v} \approx 0.8\,\mathrm{ms}^{-1}$, $l \approx 100\,\mathrm{m}$), we can estimate the maximal kinetic potential gradient to be about $10\,\mathrm{Pa\,m}^{-1}$, which is a factor 40 smaller than the measured pressure gradient plus the elevation potential gradient (Fig. 3a), and six times smaller than the 15% error on that quantity. Similarly for AM15, using $\bar{v} \approx 2\,\mathrm{ms}^{-1}$, $l \approx 50\,\mathrm{m}$, gives a maximal estimated kinetic potential gradient of about $40\,\mathrm{Pa\,m}^{-1}$, which is a factor 20 smaller than the measured pressure gradient plus the elevation potential gradient and three times smaller than the standard error on that quantity. Therefore it is appropriate to neglect the kinetic potential in our derivations.

ESTIMATION OF CLOSURE RATE

In general, the evolution of the cross-sectional area S of an R-channel is described as

$$\frac{\partial S}{\partial t} = v_o - v_c, \tag{S3}$$

which is the balance between the opening rate v_o and the closure rate v_c. In our study we only consider v_o and set $v_c \approx 0$. Here we show that v_c is in fact negligible.

The closure rate v_c is the result of viscous deformation of ice and commonly formulated in terms of Glen's flow law

$$v_c = \frac{2}{n^n} A \, S |N|^{n-1} N, \tag{S4}$$

where $A = 2.4 \times 10^{-24}\,s^{-1}\,\mathrm{Pa}^{-3}$ (at $0\,^\circ\mathrm{C}$, e.g. Cuffey and Paterson (2010)) and $n = 3$ are empirical coefficients associated to Glen's flow law and N is the effective pressure

$$N = p_i - p_w = \rho_i g z + p_{atm} - p_w, \tag{S5}$$

with p_i being the hydrostatic ice pressure of an ice column of thickness z, p_w the water pressure, ρ_i the ice density, g the gravitational acceleration and p_{atm} the atmospheric pressure that we measured with the stage sensor (uncertainty of 50 Pa). For z we use the mean depth of the two sensors (Table S1) and for p_w the mean between the values measured by these two sensors (see Fig. S2).

In the time series of 9 and 21 of August 2020 (referred to as 9-Aug/AM15 and 21-Aug/AM13, respectively), for which we run the c_t-gradient model and the free-gradient model, the closure rates are always negligible compared to the opening rates (Figs. S3 and S4, Table S3). For 9-Aug/AM15, the opening rates as determined by the c_t-gradient model and the free-gradient model are in the order of $\sim 10^{-6}\,\mathrm{m}^2\,\mathrm{s}^{-1}$. The closure rates, determined through Eq. (S4), vary between $10^{-14}\,\mathrm{m}^2\,\mathrm{s}^{-1}$ and $10^{-9}\,\mathrm{m}^2\,\mathrm{s}^{-1}$. This means that the closure rates are always at least three orders of magnitude smaller than the opening rates. For 21-Aug/AM13, the opening rates are in the order of $\sim 10^{-7}\,\mathrm{m}^2\,\mathrm{s}^{-1}$ while the closure rates are around $\sim -10^{-11}\,\mathrm{m}^2\,\mathrm{s}^{-1}$, or four orders of magnitude smaller in their absolute value. The negative closure rates on this day mean that the water pressure was larger than the ice overburden pressure.

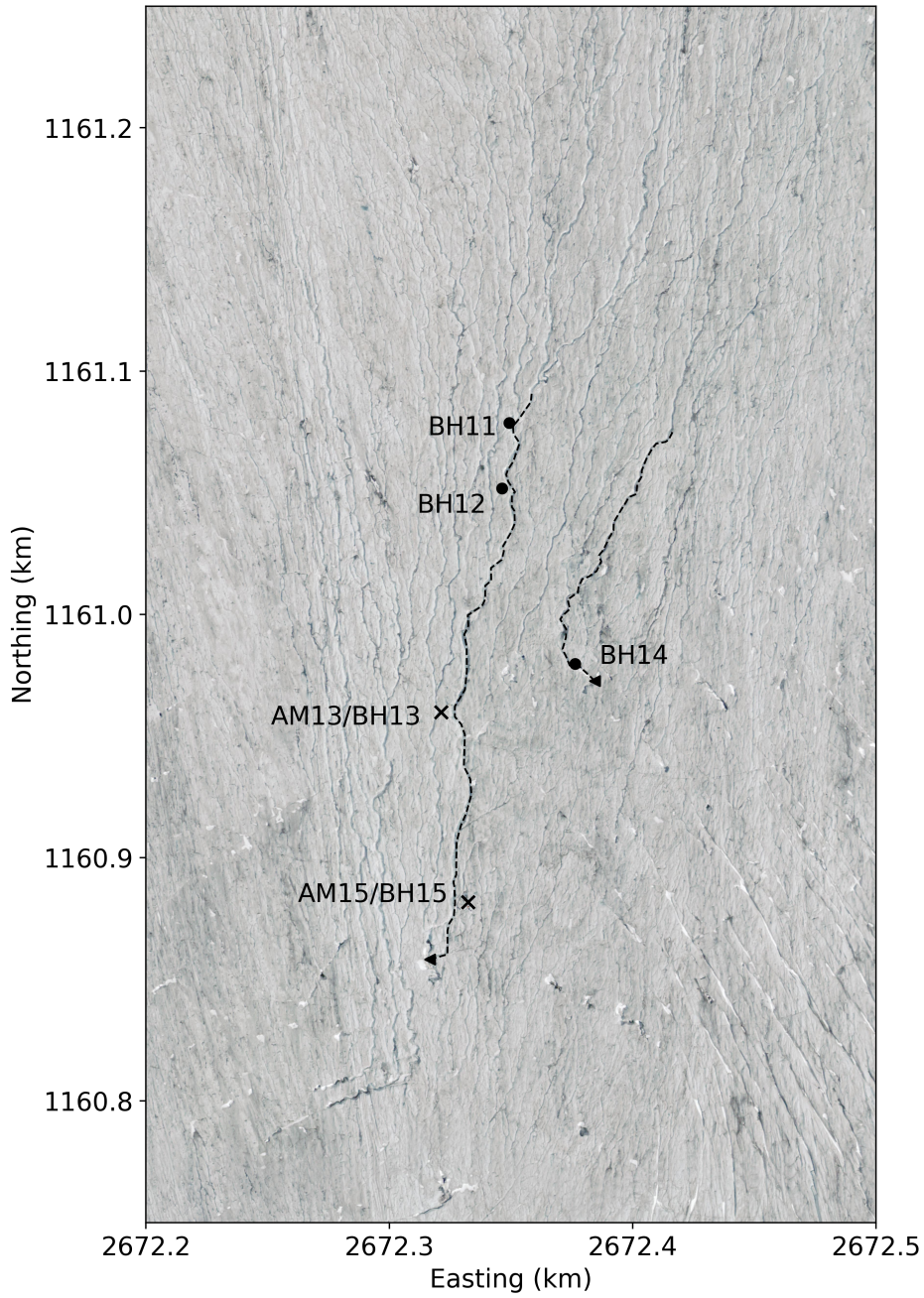

Fig. S1. Ortho-rectified aerial image of the field site including the locations of the main streams, boreholes and artificial moulins (as also shown in Fig. 1). Note that this is a high-resolution image and will reveal many details when zoomed in (data from swisstopo).

FITTING THE FREE-GRADIENT MODEL

In each iteration of the MCMC procedure, the free-gradient model simulates the cross-sectional area $\hat{\mathbf{S}}(\mathbf{m})$ based on model parameters $\mathbf{m} = [\partial T_w/\partial z, \hat{S}_0]$, where $\hat{S}_0$ is the initial condition for the cross-sectional area. The posterior probability function $P(\mathbf{m}|\mathbf{d})$ then describes the agreement with the data of the cross-sectional area $\mathbf{d}$:

$$P(\mathbf{m}|\mathbf{d}) \propto P(\mathbf{d}|\mathbf{m})P(\mathbf{m}), \tag{S6}$$

where $P(\mathbf{d}|\mathbf{m})$ and $P(\mathbf{m}) = P(\partial T_w/\partial z)P(\hat{S}_0)$ are the priors in data and model space, respectively; the former is commonly called the likelihood. For $P(\mathbf{d}|\mathbf{m})$ and $P(\hat{S}_0)$ we use Gaussian distributions with the propagated uncertainties as the standard deviations assuming independent measurements; for $P(\partial T_w/\partial z)$ we use a uniform distribution:

$$P(\mathbf{d}|\mathbf{m}) \propto \exp\left[-\frac{1}{2}\sum_{i=1}^{M}\left(\frac{|\hat{S}_i(\mathbf{m}) - d_i|}{\sigma_i}\right)^2\right], \tag{S7}$$

$$P(\hat{S}_0) \propto \exp\left[-\frac{1}{2}\left(\frac{|\hat{S}_0 - d_0|}{\sigma_0}\right)^2\right], \tag{S8}$$

$$P(\partial T_w/\partial z) \propto \begin{cases} 1, & \text{if } \partial T_w/\partial z \in [-10^{-2}, -10^{-6}]\,\mathrm{K\,m^{-1}} \\ 0, & \text{otherwise.} \end{cases} \tag{S9}$$

d_i is the ith of the $M-1$ measured cross-sectional areas with uncertainty σ_i and the corresponding model output $\hat{S}_i(\mathbf{m})$.

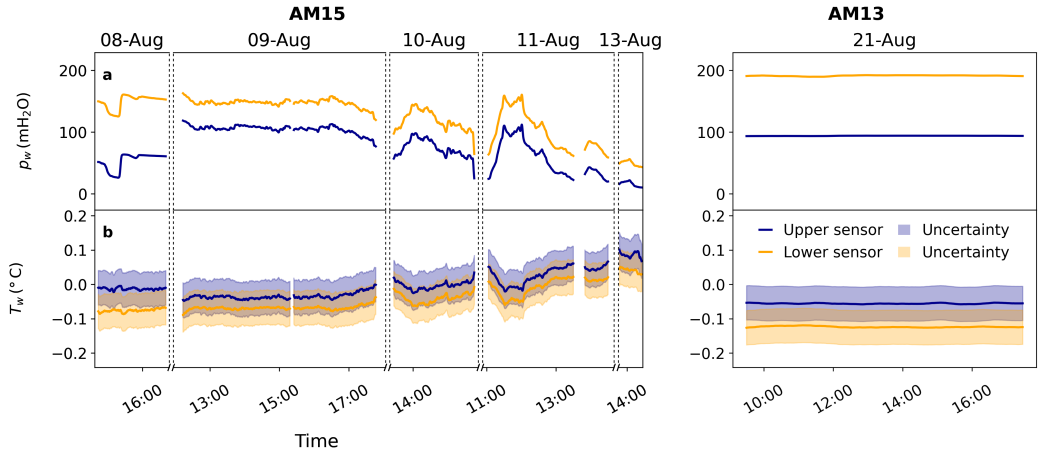

Fig. S2. (a) water pressure p_w and (b) water temperature T_w, measured by the two CTDs in artificial moulin AM15 (left) and AM13 (right). The plotted time spans are the same as in Figure 3 in the main document. They represent the time spans when we conducted tracer experiments and when the flow was pressurised. When comparing p_w between different days, note that the depths of the sensors and the length of the test-section (their vertical distance) were not always the same (see Table S1).

Table S1. Depth of the two CTDs on the days where the condition of pressurised flow between the sensors was met. It is always constant over the course of one day. Upper and lower CTD always refer to the same instruments, they were never exchanged or switched during the field campaign.

Day	Test-section length (m)	CTD depth (m)	
		Upper	Lower
AM15			
08 August 2020	102.2	62.4	164.6
09 August 2020	50.6	121.1	171.7
10 August 2020	50.8	120.9	171.7
11 August 2020	50.7	121.0	171.7
13 August 2020	40.3	131.6	171.9
AM13			
21 August 2020	101.5	88.4	189.9

DERIVING EQUILIBRIUM TEMPERATURE AND ITS LENGTH-SCALE

Here we derive both the equilibrium temperature of water flowing in an R-channel and the equilibrating length scale associated with reaching it. The result will be similar to eq. 29 of Sommers and Rajaram (2020) but also includes effects given by the pressure-melting point.

The steady-state energy equation is given by

$$v\frac{dE}{dz} = M, \tag{S10}$$

where $dE/dz = \rho_w c_w S dT_w/dz$ is the thermal energy gradient ($\mathrm{J\,m^{-1}}$), z the distance along channel-flow path (m), v the stream flow velocity ($\mathrm{m\,s^{-1}}$, assumed constant in space), and M is a source term ($\mathrm{W\,m^{-1}}$). The source is composed of potential energy dissipation and heat flux into the channel wall (melting the ice there)

$$M = -Q\frac{d\phi}{dz} - P_w H(T_w - T_i), \tag{S11}$$

where $T_i = c_t p_w$ is the ice temperature at the pressure melting point (° C), $P_w = 2\sqrt{\pi S}$ the wetted perimeter (m), and H the heat transfer coefficient ($\mathrm{W\,m^{-2}\,K^{-1}}$). Inserting this into Eq. (S10) and divding by $P_w H$ yields

$$z_0\frac{dT_w}{dz} = -\frac{Q}{P_w H}\frac{d\phi}{dz} - (T_w - c_t p_w), \tag{S12}$$

with the equilibrating (e-folding) length scale defined as

$$z_0 = \frac{\rho_w c_w Q}{P_w H}. \tag{S13}$$

To solve this we define $\tau_w = T_w - c_t p_w$, the offset of the water temperature from the pressure melting point, and do a variable substitution

$$z_0\frac{d\tau_w}{dz} = -\frac{Q}{P_w H}\frac{d\phi}{dz} - z_0 c_t\frac{dp_w}{dz} - \tau_w. \tag{S14}$$

Defining the equilibrium temperature (given as offset from the melting point) as

$$\tau_{eq} = -\frac{Q}{P_w H}\left(\frac{d\phi}{dz} + \rho_w c_w c_t\frac{dp_w}{dz}\right), \tag{S15}$$

shows that τ_{eq} is the energy available for melt (see Eq. (12) of the main document) scaled by $P_w H$.

Equation (S14) now reads

$$z_0\frac{d\tau_w}{dz} = \tau_{eq} - \tau_w. \tag{S16}$$

We can integrate this equation, assuming that Q, P_w, $\frac{d\phi}{dz}$, $\frac{dp_w}{dz}$, and thus τ_{eq} are constant, which should be approximately true for a uniformly inclined channel. Expressed in terms of offset temperatures from the melting point, the solution is

$$\tau_w(z) = \tau_{eq} + (\tau_{w0} - \tau_{eq})\exp\left(\frac{-z}{z_0}\right), \tag{S17}$$

where τ_{w0} is water temperature at $z = 0$. In terms of absolute temperatures (°C):

$$\begin{aligned} T_w(z) = {} & c_t p_w \\ & + (T_{w0} - c_t p_w)\exp\left(\frac{-z}{z_0}\right) \\ & + (T_{eq} - c_t p_w)\left(1 - \exp\left(\frac{-z}{z_0}\right)\right), \end{aligned} \tag{S18}$$

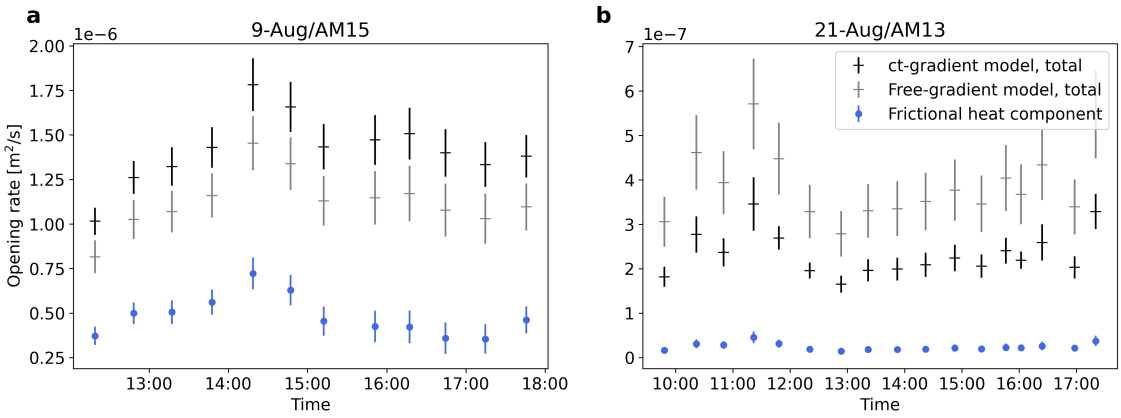

Fig. S3. Opening rates according to the c_t-gradient model (black) and the free-gradient model (blue) in the time series for (a) 9-Aug/AM15, and (b) 21-Aug/AM13. The fraction of the opening rates that is caused by frictional heating is indicated in grey and is the same for both models. The difference between total opening rates and the frictional heat component corresponds to the energy provided by sensible heat, which differs between the two models. Uncertainties at one standard deviation are represented by vertical lines.

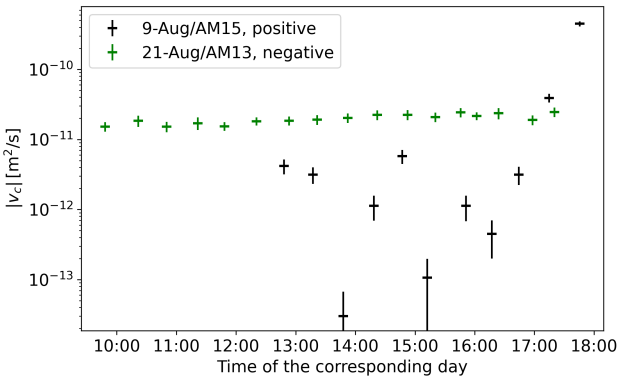

Fig. S4. Absolute values of closure rates computed for the time series of AM15 on 9 August (9-Aug/AM15, black) and for AM13 on 21 August (21-Aug/AM13, green). The closure rates themselves are all positive for 9-Aug/AM15 and negative for 21-Aug/AM13.

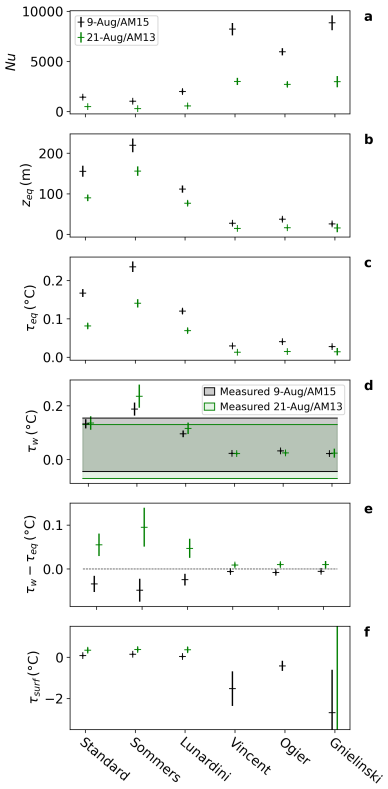

Fig. S5. As Figure 5 in the main document, but additionally with panel (f) showing the expected offset-temperatures at the surface. Vincent, Ogier and Gnielinski values are not or only partly shown since they are above 100 °C for 21-Aug/AM13 (see Tab. S2)

with $T_{eq} = \tau_{eq} + c_t p_w$. Note that Eq. (S17) reduces to eq. 29 of Sommers and Rajaram (2020) for $c_t = 0$.

The Nusselt number

Most terms of Eq. (S14) are derived from measurements or estimated from the free-gradient model. The only missing variables is the heat transfer coefficient H which can be expressed in terms of the Nusselt number Nu:

$$Nu = \frac{HD}{k}. \tag{S19}$$

Here, $k = 0.57\,\mathrm{Wm^{-1}\,°C^{-1}}$ is the thermal conductivity of water and D is a length scale for which we take the standard value of the (hydraulic) diameter $D = 2\sqrt{S/\pi}$. For Nu there are a number of empirical parameterisations available; for each we calculate τ_w. We then compare each τ_w to our temperature measurements and can check which parameterisations are compatible with our data.

In the main document, we show daily means of the thermodynamic properties (Fig. 5). Here, in Figure S5f, we additionally show the predicted surface offset-temperature τ_{surf} and list all values in Table S2. In Figure S6 the results corresponding to individual tracer experiments are resolved, which shows that the variation between different Nu parameterisations is larger than the variations within one day.

REFERENCES

Clarke GKC (2003) Hydraulics of subglacial outburst floods: new insights from the Spring-Hutter formulation. *Journal of Glaciology*, **49**(165), 299–313 (doi: 10.3189/172756503781830728)

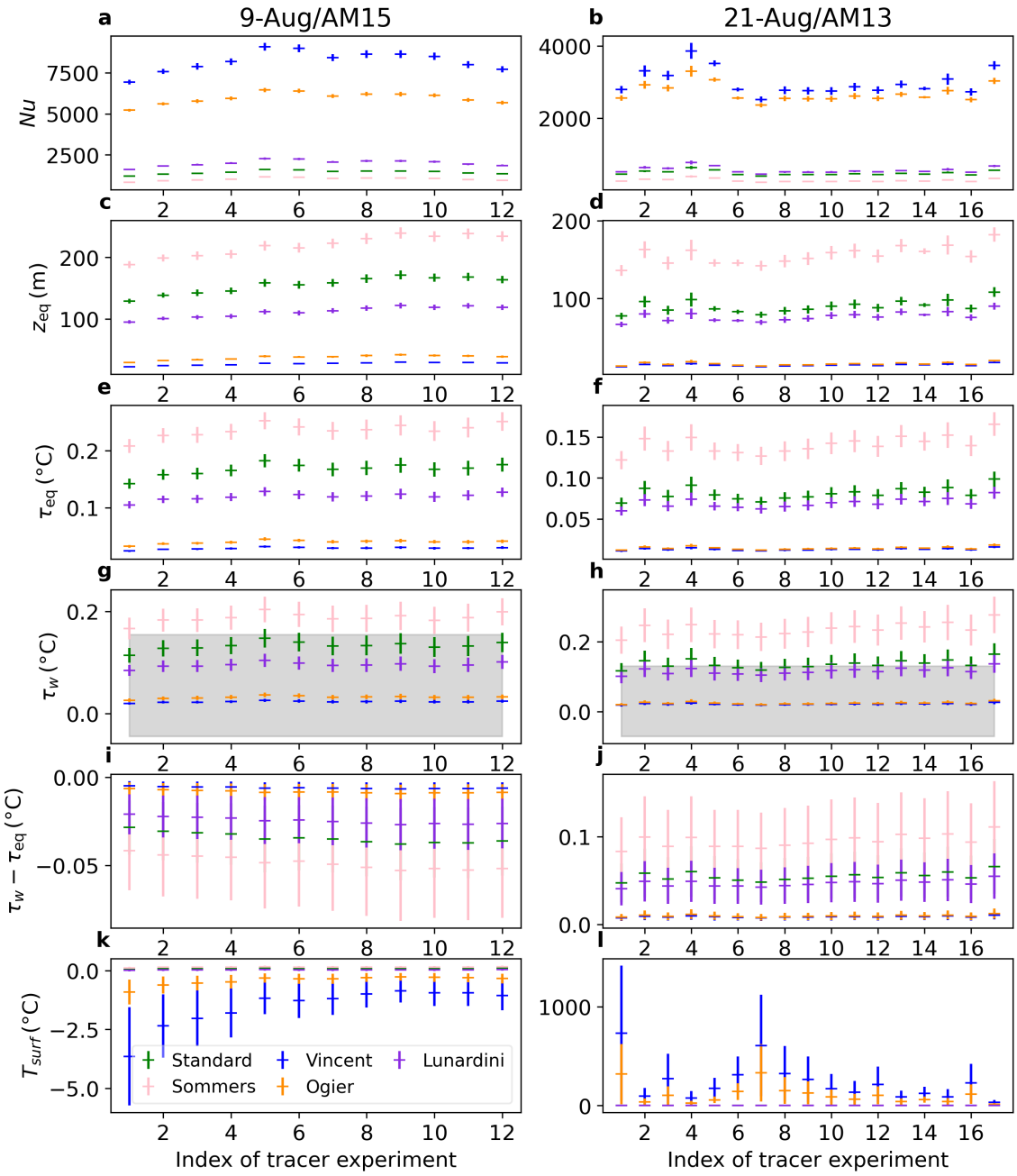

Fig. S6. Parameters as in Figures 5 (main document) and S5 but showing values of individual tracer experiments rather than daily means.

Cuffey KM and Paterson WSB (2010) *The physics of glaciers*. Elsevier, Amsterdam, fourth edition

Nye JF (1976) Water flow in glaciers: jökulhlaups, tunnels and veins. *Journal of Glaciology*, **17**(76), 181–207 (doi: 10.3189/s002214300001354x)

Röthlisberger H (1972) Water pressure in intra– and subglacial channels. *Journal of Glaciology*, **11**(62), 177–203 (doi: 10.1017/cbo9780511667015.003)

Sommers AN and Rajaram H (2020) Energy transfer by turbulent dissipation in glacial conduits. *Journal of Geophysical Research: Earth Surface*, **125**(10), e2019JF005502 (doi: 10.1029/2019JF005502)

Table S2. Thermodynamic variables plotted in Figure 5 (see also Table 1). Normal font for 9-Aug/AM15, **bold**: 21-Aug/AM13

Parameter	Standard	Sommers	Lunardini	Vincent	Ogier	Gnielinski
Nu	1430.0 ± 120.0	1020.0 ± 99.0	2000.0 ± 190.0	8220.0 ± 620.0	5960.0 ± 360.0	8860.0 ± 740.0
	481.0 ± 62.0	**279.0 ± 43.0**	**565.0 ± 85.0**	**2990.0 ± 360.0**	**2700.0 ± 250.0**	**2980.0 ± 560.0**
z_{eq} (m)	155.0 ± 13.0	219.0 ± 17.0	111.0 ± 8.8	27.1 ± 2.5	37.4 ± 3.8	25.5 ± 4.0
	89.9 ± 7.8	**156.0 ± 12.0**	**76.7 ± 5.8**	**14.5 ± 1.4**	**16.0 ± 1.8**	**15.8 ± 11.0**
τ_{eq} (°C)	0.167 ± 0.01	0.236 ± 0.014	0.12 ± 0.007	0.029 ± 0.002	0.04 ± 0.003	0.027 ± 0.003
	0.081 ± 0.007	**0.141 ± 0.011**	**0.069 ± 0.005**	**0.013 ± 0.001**	**0.014 ± 0.002**	**0.014 ± 0.01**
τ_w (°C)	0.133 ± 0.017	0.187 ± 0.024	0.095 ± 0.012	0.023 ± 0.003	0.032 ± 0.004	0.022 ± 0.003
	0.136 ± 0.025	**0.235 ± 0.043**	**0.116 ± 0.021**	**0.022 ± 0.004**	**0.024 ± 0.004**	**0.024 ± 0.016**
$\tau_w - \tau_{eq}$ (°C)	-0.034 ± 0.018	-0.048 ± 0.026	-0.025 ± 0.013	-0.006 ± 0.003	-0.008 ± 0.004	-0.006 ± 0.003
	0.055 ± 0.025	**0.095 ± 0.044**	**0.047 ± 0.022**	**0.009 ± 0.004**	**0.01 ± 0.005**	**0.01 ± 0.008**
τ_{surf} (°C)	0.079 ± 0.045	0.141 ± 0.047	0.028 ± 0.047	-1.52 ± 0.83	-0.422 ± 0.25	-2.68 ± 2.1
	0.342 ± 0.12	**0.373 ± 0.11**	**0.36 ± 0.13**	**231.0 ± 190.0**	**106.0 ± 91.0**	**617.0 ± 1400.0**

Table S3. Daily means of total opening rate, opening rate due to sensible heat (without frictional dissipation), as well as closure rate. The latter is neglected in both the free-gradient model and the c_t-gradient model. Normal font: 9-Aug/AM15, **bold**: 21-Aug/AM13

Term	c_t-gradient model	free-gradient model
Total opening rate ($m^2\,s^{-1}$)	1.42×10^{-6} ± 9.2×10^{-8}	1.13×10^{-6} ± 3.9×10^{-8}
	$\mathbf{2.33}\times10^{-7}$ ± $\mathbf{1.9}\times10^{-8}$	$\mathbf{3.89}\times10^{-7}$ ± $\mathbf{1.8}\times10^{-8}$
Opening rate due to sensible heat ($m^2\,s^{-1}$)	9.35×10^{-7} ± 8.2×10^{-8}	6.46×10^{-7} ± 3.9×10^{-8}
	$\mathbf{2.08}\times10^{-7}$ ± $\mathbf{1.8}\times10^{-8}$	$\mathbf{3.65}\times10^{-7}$ ± $\mathbf{1.8}\times10^{-8}$
Closure rate ($m^2\,s^{-1}$)	4.21×10^{-11} ± 3.8×10^{-12}	
	$\mathbf{-1.98}\times10^{-11}$ ± $\mathbf{2.5}\times10^{-12}$	